

FIG. 1. Schematics of a metal nanowire illuminated by a plane wave of wavelength λ_0 . Electric field intensity sketched on a cut through the nanowire. (a) Nearly constant electric field intensity in case of the local Drude model. (b) Radially oscillating field pattern in case of the nonlocal hydrodynamic Drude model.

permittivity at infinity. The factor $\beta = \sqrt{3/5} v_F$ relates to the Fermi velocity v_F [16].

The nonlocal material response is caused by $\mathbf{J}_{\text{hd}}(\mathbf{r}, \omega)$, which affects the permittivity function for the free electron gas. If $\beta \rightarrow 0$, then the coupled system simplifies to Maxwell's equations for the local Drude model. For an illustration of the effect of the HDM, a nanowire excited by a plane wave is sketched in Fig. 1. While, for the local Drude model, the electric field intensity inside of the nanowire is nearly constant, the electric field pattern is radially oscillating considering the HDM [see Figs. 1(a) and 1(b), respectively]. The reader is referred to [31, 32] for a detailed derivation of Eqs. (1) and (2) including the applied assumptions and approximations.

Physical scattering solutions $\mathbf{E}(\mathbf{r}, \omega_0)$ and $\mathbf{J}_{\text{hd}}(\mathbf{r}, \omega_0)$ of the coupled system can be obtained for real frequencies $\omega_0 \in \mathbb{R}$. The eigenfrequencies are defined as the complex resonance poles $\tilde{\omega}_k \in \mathbb{C}$ of the analytical continuation of $\mathbf{E}(\mathbf{r}, \omega_0)$ and $\mathbf{J}_{\text{hd}}(\mathbf{r}, \omega_0)$ into the complex plane yielding $\mathbf{E}(\mathbf{r}, \omega)$ and $\mathbf{J}_{\text{hd}}(\mathbf{r}, \omega)$, where $\omega \in \mathbb{C}$ [28]. The resonant states, also called eigenmodes, of the coupled system correspond to these eigenfrequencies.

A. Numerical methods for modal analysis

The contour integral method BEYN'S ALGORITHM [34] is applied to numerically solve the nonlinear eigenproblem [35] corresponding to the coupled system given by Eqs. (1) and (2). Contour integral methods for such problems require the definition of an integration path in the complex frequency plane which encloses the eigenfrequencies corresponding to the eigenmodes of interest.

The numerical integration along this contour projects vector fields onto the space spanned by these eigenmodes. In this way, an approximate eigenspace is constructed. Then, e.g., the methods proposed in [34, 36] apply a singular-value decomposition (SVD) to this approximate eigenspace and solve a linear eigenproblem of small dimension. The approach presented in [37] applies the Rayleigh-Ritz method to the approximate eigenspace and solves a nonlinear eigenproblem of small dimension. The common property of these methods is that they essentially require the solution of scattering problems for the integration points on the chosen contour. This is in contrast to standard approaches for solving nonlinear eigenproblems, such as the Arnoldi method, which are based on linearization of the nonprojected problems using auxiliary fields [38, 39].

For the modal expansion of scattering problems, an unconjugated scalar product can be used [29]. In this context, it is an open problem how to deal with the expansion of nonholomorphic quantities, e.g., the extinction cross section. The contour-integral-based RPE [28] allows one to perform a modal expansion without a scalar product. A solution $\mathbf{E}(\mathbf{r}, \omega_0)$ to the coupled system given by Eqs. (1) and (2) can be expanded into a weighted sum of eigenmodes yielding the coupling of the modes to specific sources $\mathbf{J}(\mathbf{r}, \omega_0)$ with $\omega_0 \in \mathbb{R}$. Cauchy's integral formula,

$$\mathbf{E}(\mathbf{r}, \omega_0) = \frac{1}{2\pi i} \oint_{C_0} \frac{\mathbf{E}(\mathbf{r}, \omega)}{\omega - \omega_0} d\omega,$$

is exploited, where $\mathbf{E}(\mathbf{r}, \omega)$, $\omega \in \mathbb{C}$, is the analytical continuation of $\mathbf{E}(\mathbf{r}, \omega_0)$ into the complex plane and C_0 is a closed integration path around ω_0 so that $\mathbf{E}(\mathbf{r}, \omega)$ is holomorphic inside of C_0 . Deforming the integration path and applying Cauchy's residue theorem yield

$$\begin{aligned} \mathbf{E}(\mathbf{r}, \omega_0) = & -\frac{1}{2\pi i} \oint_{\tilde{C}_1} \frac{\mathbf{E}(\mathbf{r}, \omega)}{\omega - \omega_0} d\omega - \dots - \frac{1}{2\pi i} \oint_{\tilde{C}_K} \frac{\mathbf{E}(\mathbf{r}, \omega)}{\omega - \omega_0} d\omega \\ & + \frac{1}{2\pi i} \oint_{C_{\text{nr}}} \frac{\mathbf{E}(\mathbf{r}, \omega)}{\omega - \omega_0} d\omega, \end{aligned}$$

where $\tilde{C}_1, \dots, \tilde{C}_K$ are contours around the eigenfrequencies $\tilde{\omega}_1, \dots, \tilde{\omega}_K$ and C_{nr} is a contour including ω_0 , the eigenfrequencies $\tilde{\omega}_1, \dots, \tilde{\omega}_K$, and no additional eigenfrequencies. The Riesz projections,

$$\tilde{\mathbf{E}}_k(\mathbf{r}, \omega_0) = -\frac{1}{2\pi i} \oint_{\tilde{C}_k} \frac{\mathbf{E}(\mathbf{r}, \omega)}{\omega - \omega_0} d\omega,$$

corresponding to $\tilde{\omega}_k$ describe the coupling of the eigenmodes to the considered source field. The field,

$$\mathbf{E}_{\text{nr}}(\mathbf{r}, \omega_0) = \frac{1}{2\pi i} \oint_{C_{\text{nr}}} \frac{\mathbf{E}(\mathbf{r}, \omega)}{\omega - \omega_0} d\omega,$$

contains nonresonant components as well as components corresponding to eigenfrequencies outside of the contour C_{nr} . For this modal expansion approach, instead of projecting random vectors as for BEYN'S ALGORITHM, the numerical integration is performed by solving the coupled system using physical source fields at the integration points.

Equations (1) and (2) are spatially discretized with the finite element method (FEM) [40, 41]. The FEM solver JCMSUITE is used to solve scattering problems. Perfectly matched layers (PMLs) are applied to realize outgoing radiation conditions [42]. High order polynomial ansatz functions and mesh refinements are used to reach a sufficient numerical accuracy [43]. We write

$$T(\omega)v = f(\omega),$$

for the coupled system given by Eqs. (1) and (2), where $T(\omega) \in \mathbb{C}^{n \times n}$ is the system matrix resulting from the FEM discretization and $v \in \mathbb{C}^n$ is the vector corresponding to $\mathbf{E}(\mathbf{r}, \omega)$ and $\mathbf{J}_{\text{hd}}(\mathbf{r}, \omega)$. The dimension n results from the spatial mesh and from the degrees of the polynomial ansatz functions of the FEM discretization. The right-hand side $f(\omega)$ corresponds to the impressed current density $\mathbf{J}(\mathbf{r}, \omega)$ and incoming source fields. In this notation, $T(\tilde{\omega}_k)\tilde{v}_k = 0$ holds for an eigenfrequency $\tilde{\omega}_k$ and an eigenmode \tilde{v}_k . Solving $T(\omega)v = f(\omega)$ with $f(\omega) \neq 0$ corresponds to solving a scattering problem.

B. Modal expansion of sesquilinear quantities

Typical physical quantities are quadratic forms associated with a sesquilinear map $q(v, v^*)$ for solution fields v and their complex conjugates v^* . Examples include the electromagnetic absorption and the electromagnetic energy flux. For two reasons, the construction of a meaningful modal expansion of sesquilinear forms $q(v, v^*)$ is not straightforward. First, the missing orthogonality $q(\tilde{v}_k, \tilde{v}_l^*) \neq 0$ yields cross terms in the expansion. Secondly, the conjugation $v^*(\omega_0)$ renders $q(v(\omega_0), v^*(\omega_0))$ nonholomorphic and the evaluation of this expression for complex eigenfrequencies $\tilde{\omega}_k$ is problematic.

To derive a modal expansion of sesquilinear quantities with well-defined expansion coefficients, we extend the framework of the RPE. The method is based on an analytical continuation of the sesquilinear form $q(v(\omega_0), v^*(\omega_0))$ from the real axis $\omega_0 \in \mathbb{R}$ into the complex plane $\omega \in \mathbb{C}$. We remark that $v^*(\omega_0)$ is the solution to $T^*(\omega_0)v^*(\omega_0) = f^*(\omega_0)$. The system matrix $T^*(\omega_0)$ and the right-hand side $f^*(\omega_0)$ have analytical continuations, which we denote by $T^\circ(\omega)$ and $f^\circ(\omega)$. Consequently, the analytical continuation of $v^*(\omega_0)$ reads as

$$v^\circ(\omega) = T^\circ(\omega)^{-1}f^\circ(\omega). \quad (3)$$

Finally, this gives the analytical continuation $q(v(\omega), v^\circ(\omega))$ into the complex plane and the modal expansion can be computed.

Note that if a solution of the coupled system given by Eqs. (1) and (2) has a pole in $\omega = \tilde{\omega}_k$, then its complex conjugate has a pole in $\omega = \tilde{\omega}_k^*$. Thus, $q(v(\omega), v^\circ(\omega))$ has poles in $\tilde{\omega}_k$ and also in $\tilde{\omega}_k^*$. This has to be taken into account for the RPE. The calculation of a modal quantity corresponding to a specific $\tilde{\omega}_k$ involves the summation of the Riesz projections for $\tilde{\omega}_k$ and $\tilde{\omega}_k^*$.

As the derivation of $v^\circ(\omega)$ is given formally, we remark, for a better physical understanding, that the complex conjugation of the system matrix and the right-hand side corresponds to solving the coupled system for $\omega = -\omega_0$ with sign-inverted radiation conditions.

III. RESONANCES OF A NANOWIRE

We consider a specific setup, a cylindrical metal nanowire which has also been investigated in the literature, to study HDM-based effects theoretically [17]. For typical nanoplasmonic applications, a quantity of interest is the extinction cross section. In the following, we first compute eigenfrequencies and eigenmodes of the nanowire. Based on this, we then investigate the extinction cross section in a modal sense, i.e., it is shown which of the eigenmodes scatter and absorb an incoming source field and which of the modes do not interact with the light source. When the nonlocal HDM is replaced by a local Drude model, only a single resonance is observed in the extinction cross section [17, 22, 31].

The investigated sodium nanowire of radius $R = 2$ nm, infinitely extended in the z direction [see Fig. 1(a)], is described by $\epsilon_\infty = 1$, $\omega_p = 8.65 \times 10^{15} \text{ s}^{-1}$, $\gamma = 0.01 \omega_p$, and $\epsilon_{\text{loc}} = \epsilon_0 \epsilon_\infty$. The Fermi velocity is given by $v_F = 1.07 \times 10^6 \text{ ms}^{-1}$. The nanowire is surrounded by free space with refractive index equal to one. The source field is a y polarized plane wave with unit amplitude propagating in the x direction. For the FEM discretization, a mesh containing about 2000 triangles with edge lengths from about 0.05 nm to 1 nm is applied. The polynomial degree of the finite elements is set to $p = 3$.

The frequency range $0.4 \omega_p < \omega < 1.4 \omega_p$ is selected for the modal analysis. To compute eigenmodes \tilde{v}_k using BEYN'S ALGORITHM, an integration contour around this range is defined. The parameters for the algorithm are $N = 160$ integration points, $l = 200$ random vectors, and, for the rank drop detection within the SVD, a tolerance of $\text{tol}_{\text{rank}} = 10^{-8}$ is chosen. The SVD and the solution of the resulting small linear eigenproblem are performed within MATLAB. We obtain 118 eigenfrequencies inside the integration contour. The imaginary parts of these eigenfrequencies are $\text{Im}(\tilde{\omega}_k) = -0.0050 \omega_p$, except for $\tilde{\omega}_1 = (0.7313 - 0.0054i)\omega_p$. We note that the eigenmodes corresponding to eigenfrequencies with $\text{Im}(\tilde{\omega}_k) = -0.0050 \omega_p$ are localized in the nanowire material, which is modeled with a constant damping γ . Other loss channels are not significant for these modes. This results in the very similar imaginary parts of the eigenfrequencies. To numerically assess the quality of the ap-

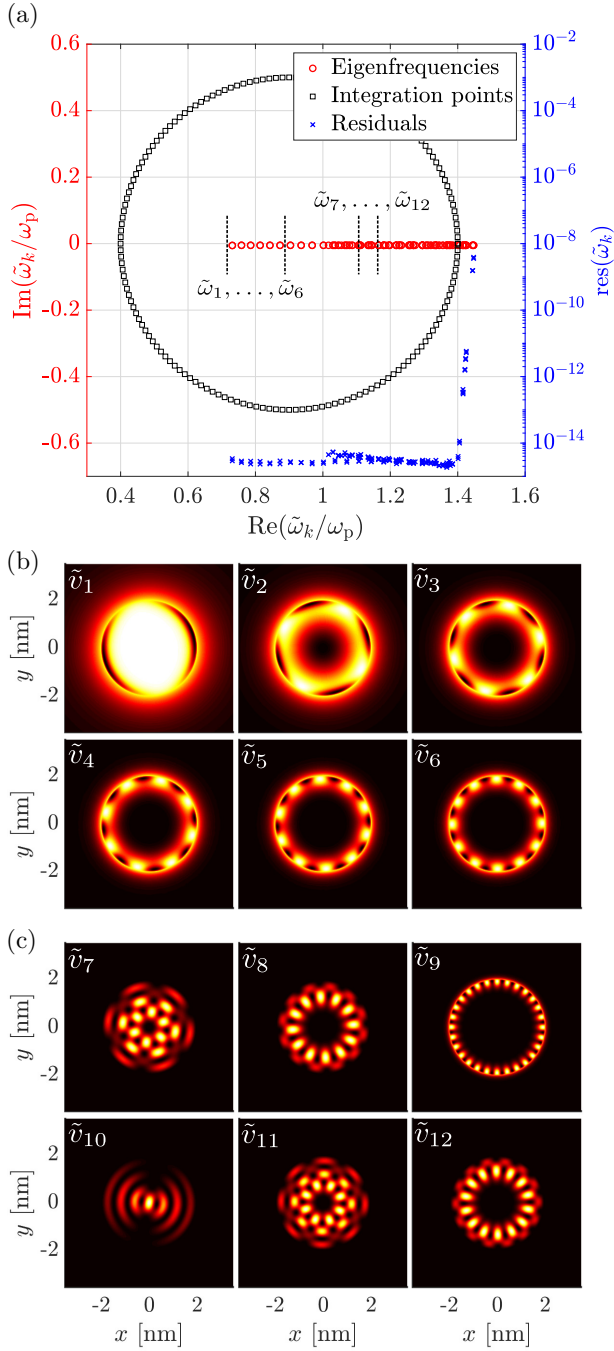


FIG. 2. Eigenfrequencies $\tilde{\omega}_k$ and eigenmodes \tilde{v}_k of the nanowire. (a) Eigenfrequencies, integration points, and residuals $\text{res}(\tilde{\omega}_k) = \|T(\tilde{\omega}_k)\tilde{v}_k\|_2 / \|T(\tilde{\omega}_k)\|_F$, where $\|\tilde{v}_k\|_2 = 1$. Inside of the integration contour, 118 eigenfrequencies are located (including multiplicities). (b) Plots (a.u.) of the electric field intensity of an exemplary selection of eigenmodes corresponding to eigenfrequencies below the plasma frequency, $\tilde{\omega}_1 = (0.7313 - 0.0054i)\omega_p$, $\tilde{\omega}_2 = (0.7585 - 0.0050i)\omega_p$, $\tilde{\omega}_3 = (0.7857 - 0.0050i)\omega_p$, $\tilde{\omega}_4 = (0.8138 - 0.0050i)\omega_p$, $\tilde{\omega}_5 = (0.8429 - 0.0050i)\omega_p$, and $\tilde{\omega}_6 = (0.8729 - 0.0050i)\omega_p$. (c) As above, for eigenfrequencies beyond the plasma frequency, $\tilde{\omega}_7 = (1.1341 - 0.0050i)\omega_p$, $\tilde{\omega}_8 = (1.1373 - 0.0050i)\omega_p$, $\tilde{\omega}_9 = (1.1434 - 0.0050i)\omega_p$, $\tilde{\omega}_{10} = (1.1453 - 0.0050i)\omega_p$, $\tilde{\omega}_{11} = (1.1651 - 0.0050i)\omega_p$, and $\tilde{\omega}_{12} = (1.1654 - 0.0050i)\omega_p$. Color scale from zero (black) to one (white).

proximations of the eigenfrequencies and eigenmodes, we compute the residuals $\text{res}(\tilde{\omega}_k) = \|T(\tilde{\omega}_k)\tilde{v}_k\|_2 / \|T(\tilde{\omega}_k)\|_F$, where $\|\tilde{v}_k\|_2 = 1$. The residuals for eigenfrequencies within the integration contour are smaller than 6×10^{-15} . The residuals for computed eigenfrequencies outside the integration contour increase with the distance to the contour. The integration points, all computed eigenfrequencies, and the residuals are shown in Fig. 2(a). Plots of the electric field intensity of an exemplary selection of eigenmodes corresponding to eigenfrequencies in frequency ranges below and beyond the plasma frequency are shown in Figs. 2(b) and 2(c), respectively. Note that these eigenfrequencies are semi-simple with an algebraic and geometric multiplicity of two. The chosen indices of the eigenfrequencies and eigenmodes are increasing with increasing real parts of the eigenfrequencies and are intended to guide the reader through the figures.

Based on the computed spectrum, we investigate the extinction cross section,

$$\sigma(\omega_0) = \frac{1}{P_{\text{pw}}} \left[\int_{\delta\Omega} \frac{1}{2} \text{Re}(\mathbf{E}^*(\mathbf{r}, \omega_0) \times \mathbf{H}(\mathbf{r}, \omega_0)) \cdot d\mathbf{S} + \int_{\Omega_{\text{nw}}} \frac{1}{2} \text{Re}(\mathbf{E}^*(\mathbf{r}, \omega_0) \cdot \mathbf{J}_{\text{hd}}(\mathbf{r}, \omega_0)) dV \right],$$

where the first term is the power flux across the boundary of the entire computational domain, denoted by $\delta\Omega$, and the second term is the energy loss in the domain where the nanowire exists, denoted by Ω_{nw} [31]. The incoming plane wave with real frequencies ω_0 is normalized so that the power flux through the geometrical cross section of the nanowire is $P_{\text{pw}} = 4 \times 10^{-9}$ W. To quantify the coupling of the light source to specific eigenmodes, the RPE is applied. This requires the holomorphic evaluation of sesquilinear quantities from Eq. (3) and yields the modal extinction cross section $\tilde{\sigma}_k(\omega_0)$ corresponding to an eigenfrequency $\tilde{\omega}_k$. The direct solution of the coupled system given by Eqs. (1) and (2) yields the total extinction cross section $\sigma_{\text{tot}}(\omega_0)$.

First, we investigate the modal extinction cross section in a small frequency range including $\tilde{\omega}_7, \dots, \tilde{\omega}_{12}$. Figure 3(a) shows $\tilde{\sigma}_7(\omega_0), \dots, \tilde{\sigma}_{12}(\omega_0)$, and $\sigma_{\text{tot}}(\omega_0)$. The eigenmode \tilde{v}_{10} has a significant contribution to $\sigma_{\text{tot}}(\omega_0)$. The contributions of the eigenmodes $\tilde{v}_7, \tilde{v}_8, \tilde{v}_9, \tilde{v}_{11}$, and \tilde{v}_{12} are negligible.

Secondly, in order to understand why a specific eigenmode couples to the incoming plane wave, a fast Fourier transform of the electric field intensities of the eigenmodes on a circle inside the nanowire is performed. This yields the number of intensity maxima along the boundary of the nanowire, which we denote by $n_\varphi(\tilde{\omega}_k)$. In this way, it is possible to classify the eigenmodes. Figure 3(b) shows $n_\varphi(\tilde{\omega}_k)$ for the frequency range $0.4\omega_p < \text{Re}(\tilde{\omega}_k) < 1.4\omega_p$. The field intensities of the six eigenmodes with $n_\varphi(\tilde{\omega}_k) = 2$ are plotted in Fig. 3(c). It can be seen that these modes are dipolelike. Due to the relation of the radius of the nanowire and the wavelength of the plane wave, $R \ll \lambda_0$, the overlap integral of source

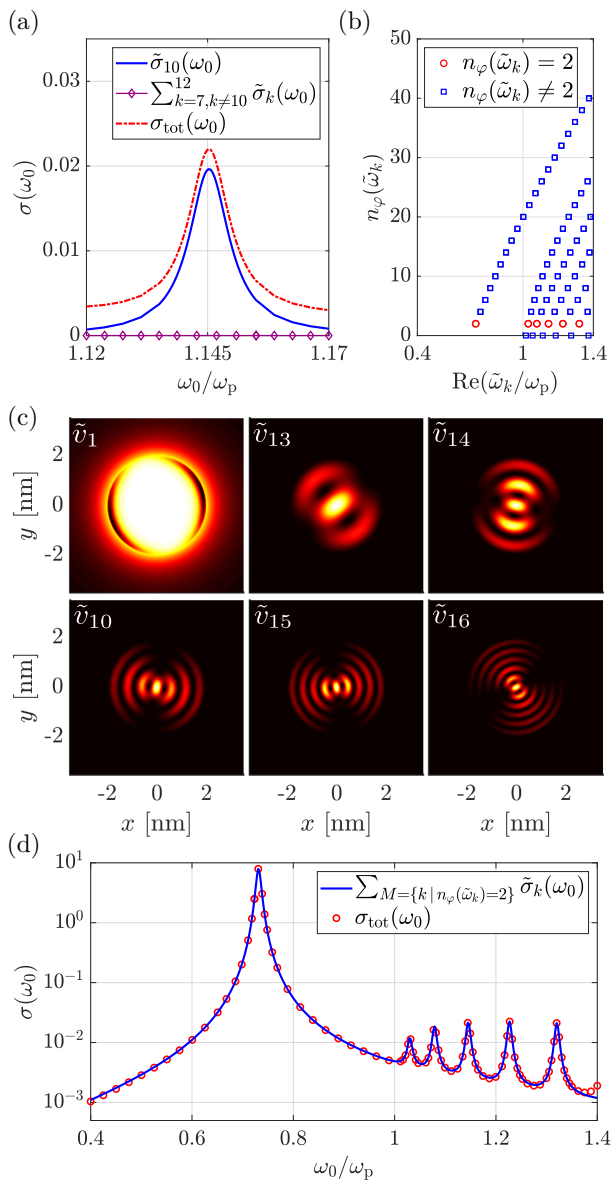


FIG. 3. Modal analysis of the extinction cross section $\sigma(\omega_0)$ of the nanowire. (a) $\sigma(\omega_0)$ for the frequency range $1.12\omega_p < \omega_0 < 1.17\omega_p$. Modal extinction cross section $\tilde{\sigma}_{10}(\omega_0)$ corresponding to the eigenfrequency $\tilde{\omega}_{10} = (1.1453 - 0.0050i)\omega_p$ and the sum $\sum_{k=7, k \neq 10}^{12} \tilde{\sigma}_k(\omega_0)$ corresponding to the remaining eigenfrequencies in the frequency range. Total extinction cross section $\sigma_{\text{tot}}(\omega_0)$ for comparison. (b) Classification parameter $n_\varphi(\tilde{\omega}_k)$ for the eigenfrequencies $\tilde{\omega}_k$ in the frequency range $0.4\omega_p < \text{Re}(\tilde{\omega}_k) < 1.4\omega_p$. (c) Plots (a.u.) of the electric field intensities of the eigenmodes with $n_\varphi(\tilde{\omega}_k) = 2$. Color scale from zero (black) to one (white). (d) Modal expansion of the extinction cross section $\sum_M \tilde{\sigma}_k(\omega_0)$, $M = \{k | n_\varphi(\tilde{\omega}_k) = 2\}$, corresponding to the six eigenfrequencies $\tilde{\omega}_1 = (0.7313 - 0.0054i)\omega_p$, $\tilde{\omega}_{13} = (1.0301 - 0.0050i)\omega_p$, $\tilde{\omega}_{14} = (1.0788 - 0.0050i)\omega_p$, $\tilde{\omega}_{10} = (1.1453 - 0.0050i)\omega_p$, $\tilde{\omega}_{15} = (1.2267 - 0.0050i)\omega_p$, and $\tilde{\omega}_{16} = (1.3202 - 0.0050i)\omega_p$. The total extinction cross section $\sigma_{\text{tot}}(\omega_0)$ is plotted as a reference solution.

field and eigenmode field has a significant contribution only for these modes.

Finally, the modal extinction cross sections $\tilde{\sigma}_k(\omega_0)$ for the eigenfrequencies with $n_\varphi(\tilde{\omega}_k) = 2$ are computed. Figure 3(d) shows the sum of the modal extinction cross sections $\sum_M \tilde{\sigma}_k(\omega_0)$, $M = \{k | n_\varphi(\tilde{\omega}_k) = 2\}$. For the investigated scattering of a plane wave, the agreement of the expansion with the total extinction cross section $\sigma_{\text{tot}}(\omega_0)$ demonstrates that the complex scattering behavior of the HDM-based nanowire is governed by a few eigenmodes only. Note that the total extinction cross section is in agreement with results from the literature [17, 31].

For illumination with different types of source fields, e.g., dipole sources, also the remaining eigenmodes of the rich spectrum can be excited.

IV. CONCLUSIONS

We investigated the light-matter interaction in nanoplasmonic systems described by the HDM. We presented a contour-integral-based framework for modal analysis, which enables the direct computation of the spectrum of nonlocal material systems. We introduced an approach for the modal expansion of sesquilinear quantities. This opens the possibility to investigate typical physical observables, e.g., the energy flux, the energy absorption, and overlap integrals for extraction efficiencies. Due to the generality of this approach, we expect that it will prove useful also in other fields of physics. Resonant states and the modal extinction cross section of a metal nanowire were calculated. While the spectrum of this system consists of many eigenfrequencies, only a few resonant states have a significant contribution to the extinction cross section. These resonant states were identified and used to expand the quantity of interest.

As demonstrated, nanoplasmonic systems on small length scales exhibit a large number of additional resonant states described by the HDM. A typical feature of these states is their high local field energy concentration. With precisely defined source fields, specific states can be excited. We expect that this will allow for additional degrees of freedom in tailoring light-matter interactions. A modal picture is a prerequisite for the understanding and for the design of corresponding nanoplasmonic devices.

ACKNOWLEDGEMENTS

We acknowledge Philipp-Immanuel Schneider and Fridtjof Betz for fruitful discussions. We acknowledge funding by the Deutsche Forschungsgemeinschaft under Germany's Excellence Strategy - The Berlin Mathematics Research Center MATH+ (EXC-2046/1, Project No. 390685689, AA4-6). This work is partially funded through the project 17FUN01 (BeCOME) within the Programme EMPIR. The EMPIR initiative is co-founded by the European Union's Horizon 2020 research and innovation program and the EMPIR Participating Countries.

-
- [1] N. C. Lindquist, P. Nagpal, K. M. McPeak, D. J. Norris, and S.-H. Oh, *Rep. Prog. Phys.* **75**, 036501 (2012).
- [2] R. F. Oulton, V. J. Sorger, T. Zentgraf, R.-M. Ma, C. Gladden, L. Dai, G. Bartal, and X. Zhang, *Nature* **461**, 629 (2009).
- [3] A. G. Curto, G. Volpe, T. H. Taminiau, M. P. Kreuzer, R. Quidant, and N. F. van Hulst, *Science* **329**, 930 (2010).
- [4] V. Giannini, A. I. Fernández-Domínguez, S. C. Heck, and S. A. Maier, *Chem. Rev.* **111**, 3888 (2011).
- [5] S. Nie and S. R. Emory, *Science* **275**, 1102 (1997).
- [6] Y. Zhang, S. He, W. Guo, Y. Hu, J. Huang, J. R. Mulcahy, and W. D. Wei, *Chem. Rev.* **118**, 2927 (2018).
- [7] R. Chikkaraddy, B. de Nijs, F. Benz, S. J. Barrow, O. A. Scherman, E. Rosta, A. Demetriadou, P. Fox, O. Hess, and J. J. Baumberg, *Nature* **535**, 127 (2016).
- [8] W. A. Murray and W. L. Barnes, *Adv. Mater.* **19**, 3771 (2007).
- [9] H. S. Sehmi, W. Langbein, and E. A. Muljarov, *Phys. Rev. B* **95**, 115444 (2017).
- [10] M. Garcia-Vergara, G. Demésey, and F. Zolla, *Opt. Lett.* **42**, 1145 (2017).
- [11] P. B. Johnson and R. W. Christy, *Phys. Rev. B* **6**, 4370 (1972).
- [12] S. Raza, S. I. Bozhevolnyi, M. Wubs, and N. A. Mortensen, *J. Phys. Condens. Matter* **27**, 183204 (2015).
- [13] J. A. Scholl, A. L. Koh, and J. A. Dionne, *Nature* **483**, 421 (2012).
- [14] S. Raza, N. Stenger, S. Kadkhodazadeh, S. V. Fischer, N. Kostesha, A.-P. Jauho, A. Burrows, M. Wubs, and N. A. Mortensen, *Nanophotonics* **2**, 131 (2013).
- [15] T. Christensen, W. Yan, S. Raza, A.-P. Jauho, N. A. Mortensen, and M. Wubs, *ACS Nano* **8**, 1745 (2014).
- [16] A. D. Boardman, *Electromagnetic Surface Modes. Hydrodynamic Theory of Plasmon-Polaritons on Plane Surfaces* (Wiley, New York, 1982).
- [17] R. Ruppin, *Opt. Commun.* **190**, 205 (2001).
- [18] S. Palomba, L. Novotny, and R. Palmer, *Opt. Commun.* **281**, 480 (2008).
- [19] F. J. Garca de Abajo, *J. Phys. Chem. C* **112**, 17983 (2008).
- [20] F. Intravaia and K. Busch, *Phys. Rev. A* **91**, 053836 (2015).
- [21] G. Toscano, J. Straubel, A. Kwiatkowski, C. Rockstuhl, F. Evers, N. A. Mortensen, and M. Wubs, *Nat. Commun.* **6**, 7132 (2015).
- [22] O. Schnitzer, V. Giannini, S. A. Maier, and R. V. Craster, *Proc. Royal Soc. A* **472**, 20160258 (2016).
- [23] M. Moeferd, T. Kiel, T. Sproll, F. Intravaia, and K. Busch, *Phys. Rev. B* **97**, 075431 (2018).
- [24] P. T. Kristensen and S. Hughes, *ACS Photonics* **1**, 2 (2014).
- [25] P. Lalanne, W. Yan, K. Vynck, C. Sauvan, and J.-P. Hugonin, *Laser Photonics Rev.* **12**, 1700113 (2018).
- [26] C. Sauvan, J.-P. Hugonin, I. S. Maksymov, and P. Lalanne, *Phys. Rev. Lett.* **110**, 237401 (2013).
- [27] M. Kamandar Dezfouli, R. Gordon, and S. Hughes, *Phys. Rev. A* **95**, 013846 (2017).
- [28] L. Zschiedrich, F. Binkowski, N. Nikolay, O. Benson, G. Kewes, and S. Burger, *Phys. Rev. A* **98**, 043806 (2018).
- [29] W. Yan, R. Faggiani, and P. Lalanne, *Phys. Rev. B* **97**, 205422 (2018).
- [30] J. M. McMahon, S. K. Gray, and G. C. Schatz, *Phys. Rev. Lett.* **103**, 097403 (2009).
- [31] L. R. Hiremath, L. Zschiedrich, and F. Schmidt, *J. Comp. Phys.* **231**, 5890 (2012).
- [32] G. Toscano, S. Raza, A.-P. Jauho, N. A. Mortensen, and M. Wubs, *Opt. Express* **20**, 4176 (2012).
- [33] M. Kamandar Dezfouli, C. Tserkezis, N. A. Mortensen, and S. Hughes, *Optica* **4**, 1503 (2017).
- [34] W.-J. Beyn, *Linear Algebra Its Appl.* **436**, 3839 (2012).
- [35] S. Güttel and F. Tisseur, *Acta Numer.* **26**, 1 (2017).
- [36] J. Asakura, T. Sakurai, H. Tadano, T. Ikegami, and K. Kimura, *JSIAM Lett.* **1**, 52 (2009).
- [37] B. Gavin, A. Miedlar, and E. Polizzi, *J. Comput. Sci* **27**, 107 (2018).
- [38] Y. Saad, *Numerical Methods for Large Eigenvalue Problems, 2nd ed.* (SIAM, Philadelphia, 2011).
- [39] Y. Brûlé, B. Gralak, and G. Demésey, *J. Opt. Soc. Am. B* **33**, 691 (2016).
- [40] P. Monk, *Finite Element Methods for Maxwell's Equations* (Clarendon Press, Oxford, 2003).
- [41] M. Weiser, *Inside Finite Elements* (De Gruyter, Berlin, 2016).
- [42] J.-P. Berenger, *J. Comput. Phys.* **114**, 185 (1994).
- [43] P. Lalanne, W. Yan, A. Gras, C. Sauvan, J.-P. Hugonin, M. Besbes, G. Demésey, M. D. Truong, B. Gralak, F. Zolla, A. Nicolet, F. Binkowski, L. Zschiedrich, S. Burger, J. Zimmerling, R. Remis, P. Urbach, H. T. Liu, and T. Weiss, *J. Opt. Soc. Am. A* **36**, 686 (2019).